PROCEEDINGS, 45th Workshop on Geothermal Reservoir Engineering
Stanford University, Stanford, California, February 10-12, 2020
SGP-TR-216

Comparison of Surface Deformation Rates from InSAR and Ground-Based Surveys in Geothermal Fields of California

[1]Mariana Eneva, [1]David Adams, [2]Kelly Blake, [3]Vicky Hsiao and [3]Giacomo Falorni

[1]Imageair Inc., 600 Greensburg Circle, Reno, NV 89509, USA

[2]U.S. Navy Geothermal Program Office, 429 E. Bowen Road, China Lake, CA 93555, USA

[3]TRE Altamira Inc., Suite 410, 475 West Georgia Street, Vancouver, BC V6B 4M9, Canada

meneva@imageair-inc.com

Keywords: InSAR, subsidence, surface deformation, leveling, surveys, geothermal fields, Coso, Salton Sea, Heber, North Brawley, Imperial Valley

ABSTRACT

Surface vertical deformation rates obtained from InSAR (Interferometric Synthetic Aperture Radar) and ground-based surveys are compared for four geothermal fields in California: Coso, Salton Sea, Heber, and North Brawley. They are also compared with the time series of monthly production and injection provided by the California Geologic Energy Management Division (CalGEM)/California Department of Conservation. The InSAR estimates are obtained by applying the SqueeSAR technique developed by TRE Altamira Inc. to scenes from the Envisat, Sentinel, and TerraSAR-X satellites, covering various non-overlapping time periods between 2003 and 2019.

The subsidence data for the Coso geothermal field, provided by the U.S. Navy Geothermal Program Office (GPO), are available from 13 surveys since 1988, four of which have been carried out since 2006 when the satellite coverage began for this area. More than 70 GPS stations have been surveyed over this period. Both the InSAR and the subsidence surveys indicate decreasing subsidence rates with time, along with decreasing production and injection rates. Only two leveling surveys, in 2006 and 2009, were carried out during the Envisat time period for Coso (2006-2010), and only one survey, in 2017, was done during the Sentinel time period (2015-2019). For this reason, comparisons between subsidence surveys and InSAR rates strictly within the periods covered by the satellite data are characterized by significant uncertainty. For Envisat, the average difference between the InSAR and survey rates within 200 m of the GPS stations is 0.7 ± 0.3 mm/year. For Sentinel, the difference is larger, 3.1 ± 0.3 mm/year, but this is due to the decreasing subsidence with time, while the satellite period occupies the second half of the survey period used for comparison.

The leveling data for the three other geothermal fields – Salton Sea, North Brawley, and Heber in the Imperial Valley of southern California – are available annually since 1998, 2009, and 1994, respectively. They are provided by the Imperial County Department of Public Works (ICDPW). In addition to Envisat and Sentinel data for all three fields, we also investigated data from the TerraSAR-X satellite (September 2012 – September 2013) over two of the geothermal fields, Salton Sea and North Brawley. When the periods with satellite data and survey measurements closely match, average differences between the two types of measurements are mostly within ±3.5 mm/year, with standard deviations of up to 1.1 mm/year.

To our knowledge, this study is the first systematic comparison between vertical deformation rates from InSAR and ground-based surveys in geothermal fields of California. Such comparisons make it possible to evaluate to what extent ground-based and space-based geodetic measurements in geothermal fields agree with each other. This is important because at present, InSAR measurements are available tens of times within a year, while the leveling surveys are conducted at most once per year (Imperial Valley) and once every three or more years (Coso).

1. INTRODUCTION

Surface deformation is a common occurrence in geothermally producing areas. When such operations take place in tectonically active areas, surface displacements are due to both natural and anthropogenic effects. Monitoring of surface deformation presents possibilities for reservoir management and planning, tracing subsurface fluid flow, and mitigating impact where it is important, such as in the agricultural areas of Imperial Valley in southern California. Understanding these factors can inform geothermal operators about the extent and subsurface characteristics of geothermal resources, the effect of particular combinations of production and injection amounts and locations, and planning of modifications as needed.

We have extensively reported on surface deformation monitoring using satellite data for geothermal fields in California – Coso (Eneva et al., 2018; Blake et al., 2020), Salton Sea (Eneva et al., 2009, 2012, 2013a, 2014; Barbour et al. 2016), Heber (Eneva et al., 2013b, 2019a), and North Brawley (Eneva et al., 2019b) (Figures 1 and 2). These fields will be further referred to as Coso, SSGF, HBGF, and NBGF. Where necessary, the abbreviations SSGF-CE and SSGF-ES will be used to distinguish between the CalEnergy units of the Salton Sea geothermal field (10 power plants), and its northeastern portion where EnergySource operates the J. L. Featherstone power

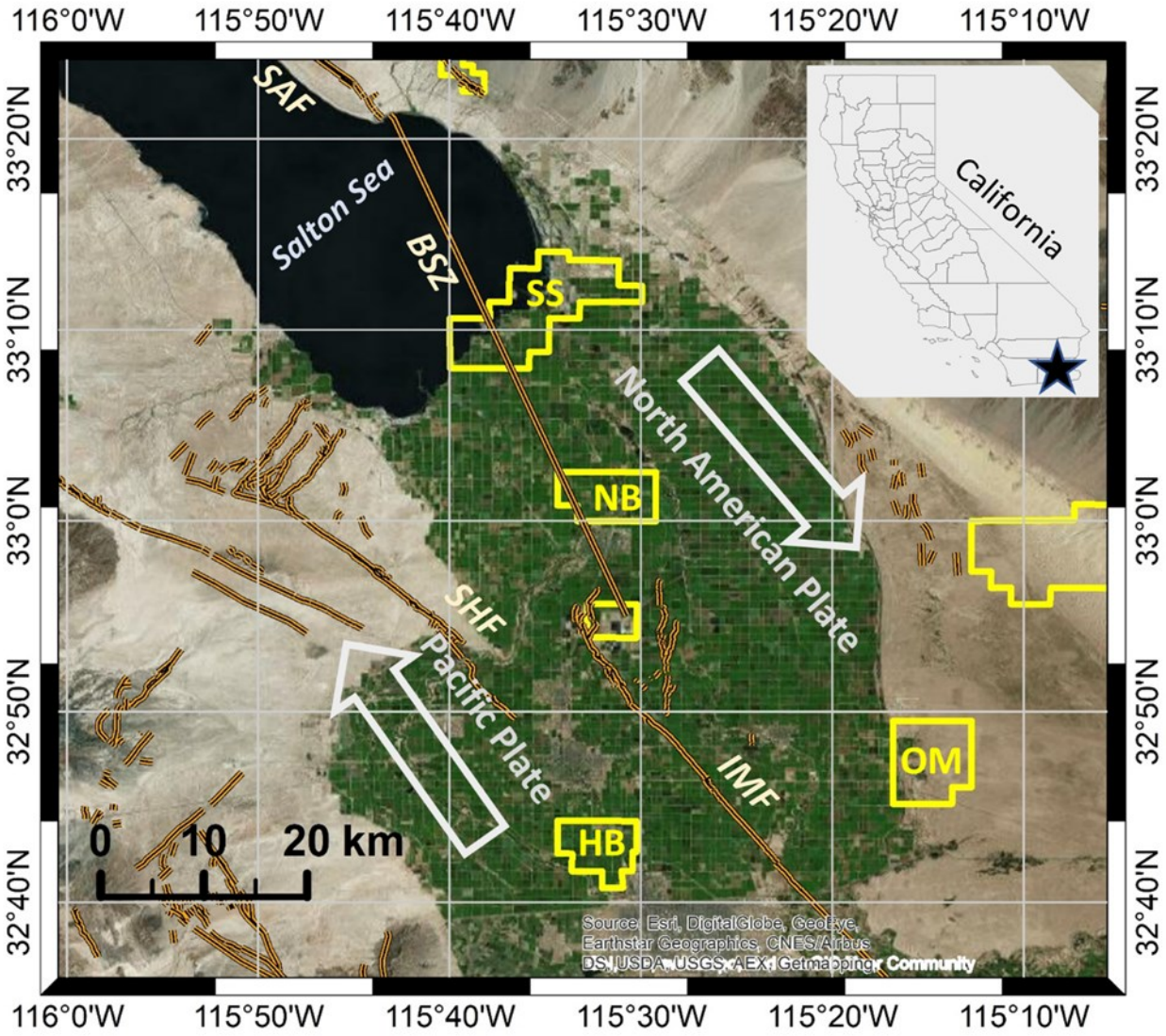

Figure 1. Map of Imperial Valley in southern California. Yellow polygons mark known geothermal resource areas (KGRAs), and yellow letters denote operating geothermal fields: SS – Salton Sea, NB – North Brawley, HB – Heber, and OM – Ormesa (also known as East Mesa). Orange lines mark faults: IMF – Imperial fault, SAF – San Andreas fault, SHF – Superstition Hills Fault, BSZ – the middle line of the Brawley Seismic Zone. Arrows mark the realtive motion of the North American and Pacific plates. Inset shows the state of California, with black star marking the location of the map.

plant (formerly known as Hudson Ranch I). Although we have previously made some comparisons with data from subsidence surveys at Coso (using GPS stations to monitor elevations) and leveling surveys in Imperial Valley (using benchmarks), a systematic comparison between the two types of measurements has not been provided. Therefore, the purpose of this paper is to report on results from such comparisons at the four geothermal fields.

The generic method used to provide observations of time series and rates of surface deformation using satellite data is InSAR (Interferometric Synthetic Aperture Radar) that has been extensively described in the literature. The specific technique we use is SqueeSAR developed at TRE Altamira Inc. (Ferretti et al., 2011). It is a state-of-the-art technique that makes use of "permanent" and "distributed" scatterers (PS and DS). The PS points can be buildings, well pads, points along roads and canals, fences, lamp posts, transmission towers, rock outcrops, etc. They serve as reflectors of the radar waves that are consistently identified in a sequence of radar scenes, so that time series of surface deformation are derived at each individual PS. The DS are homogeneous areas emitting signals with smaller signal-to-noise ratios than the PS, but still significantly above the background noise. They can be rangelands, pastures, and bare earth, characteristic of relatively arid environments and rural areas. Even in relatively dry areas, where the conventional InSAR technique works, the newer scatterer-based techniques are superior with their capability to provide time series at thousands of locations. In this paper we use the more generic term "InSAR," with which, unless stated otherwise, we mean the SqueeSAR technique.

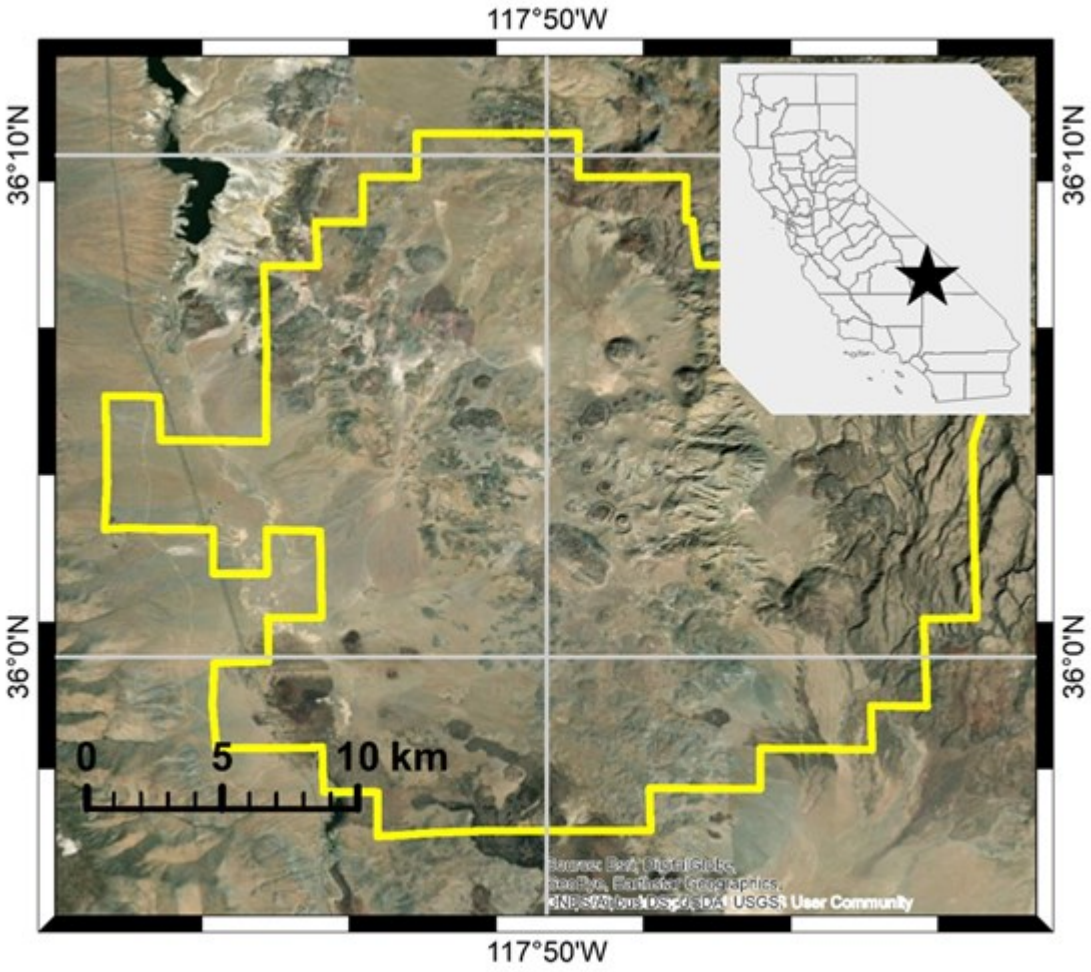

Figure 2. Map of the Coso geothermal field in the eastern part of central California. Yellow polygon marks the known geothermal resource area (KGRA). Inset shows the state of California, with black star marking the location of the map.

The deformation is measured in the line-of-sight (LOS) to the satellite, with negative and positive LOS measurements indicating movements away from and toward the satellite, respectively. Deformation time series are obtained at each PS and DS point, and are used to calculate annual deformation rates from the slopes of straight lines fitted to the time series. When these are obtained from both descending (north-to-south satellite trajectory) and ascending (south-to-north satellite trajectory) images, it is possible to decompose the two sets of LOS movements into vertical and horizontal components, calculated from the average ascending and descending LOS in pixels of a certain size (we typically use 100 m). The satellite orbital geometries of all past and current satellites with SAR instruments on board allow only the determination of the east horizontal component, while the north component cannot be resolved. The SAR instruments are right-looking, in direction perpendicular to the satellite trajectory. LOS movements are generally more sensitive to vertical displacements than to the horizontal ones, so that LOS movements away from or toward the satellite are often indicative of subsidence or uplift, respectively. For this reason, LOS and vertical deformation maps often display similar spatial patterns, even if the numerical values are different, while the east horizontal deformation maps look rather different.

Satellite data used for all geothermal fields are from the European Envisat and Sentinel satellites, covering non-overlapping periods of time, with a gap of 4 years. Envisat data are generally available for the period between Jan 2003 and Oct 2010, but the periods of data availability vary from one area to another, and also, collection of images of one type of geometry may start significantly later than the other type (e.g., ascending in the case of HBGF). The minimum frequency for the Envisat images was 35 days, due to the revisit time for any given location, but the interval between consecutive scenes could be multiples of this interval, as data were not collected during each revisit. Further in the text, Envisat data will be marked with "ENV." Sentinel data are obtained from two satellites, Sentinel-1A (launched in Apr 2014) and Sentinel-1B (launched in Apr 2016), and continue to be collected. The initial revisit time of 24 days decreased with the launch of the second Sentinel satellite, and became 12 days starting in May 2017. By now, the Sentinel revisit time is 6 days, which is significantly more frequent than the annual measurements in Imperial Valley, and the measurements at Coso once every 3-3.5 years. So far, we have processed Sentinel data twice, once until April 2018, and a second time for the period May 2018 – Aug 2019. These two Sentinel periods will be further referred to as "SNT1" and "SNT2." For the Salton Sea and North Brawley fields,

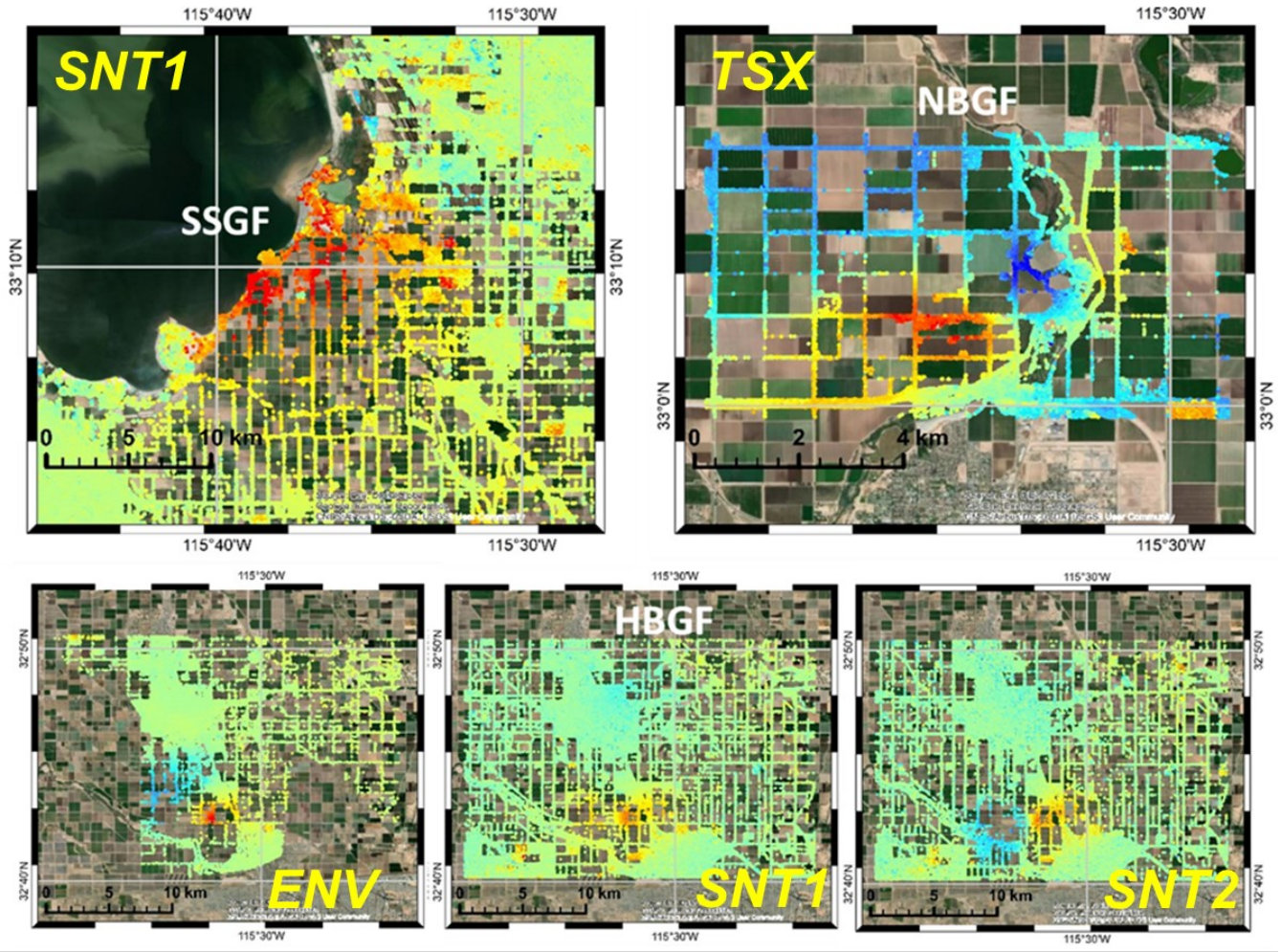

Figure 3. Examples of maps showing ascending deformation rates (mm/year) in the geothermal fields of Imperial Valley obtained from different satellites, as marked. Yellow to red colors indicate subsidence. Blue color shows uplift. Note changing pattern for HBGF.

we also have processed scenes from a high-precision German satellite, TerraSAR-X, for a one-year period, Sep 2012 – Sep 2013 (Eneva et al., 2014; Eneva et al., 2019b). These observations and the study period will be further marked with "TSX."

2. SUMMARY OF PREVIOUS AND CURRENT INSAR OBSERVATIONS

We have previously observed significant subsidence in all fields and substantial uplift in some of them (HBGF and NBGF), which vary with changes in production and injection. For example, based on ENV and SNT1 results, decreasing subsidence with time was reported for Coso by Eneva et al. (2018), from a maximum of −28 to −19 mm/year. Subsidence is also decreasing based on TSX and SNT1 observations at the NBGF (Eneva et al., 2019b), from a maximum of −39 to −15 mm/year. Continued subsidence decrease has been confirmed for both fields by the later SNT2 results. In particular, the STN2 subsidence at the NBGF is rather small, as by that time the production had become much lower than before. At HBGF, a maximum of −40 mm/year subsidence is seen in the middle of the field at all times. An uplift pattern is observed in the ENV data, to the northwest of the enduring subsidence area in the middle, with a maximum of +20 mm/year (Eneva et al., 2013b, 2019b). It transforms into subsidence in the SNT1 results (Eneva et al., 2019a), while uplift reappears in the SNT2 data to the south of the original uplift area. At Salton Sea, a maximum subsidence of −30 mm/has been observed (Eneva et al., 2014). We have also found that a significant surface deformation is present even when binary plants are used (Eneva et al., 2013a, 2019a, 2019b), despite a common assumption that because the injection fluid amounts are similar to the production ones in the binary technology, surface deformation should be greatly diminished. In fact, at a certain level of production, the maximum subsidence observed at the three geothermal fields in Imperial Valley is similar, regardless of the use of flash plants (e.g., SSGF-CE, where ~82% of the fluid is re-injected on average) or binary plants (HBGF and NBGF). However, these rates are significantly smaller than the −170 mm/year maximum rate (Sarychikhina et al., 2011) observed south of the border, at the Cerro Prieto geothermal field in Mexico, where the re-injection percentage is much lower (25% to 45%, according to unverified personal communication).

Figures 3 and 4 show examples of InSAR surface deformation rates at the four geothermal fields. While numerous PS/DS points are identified in dry areas (Coso) and urban environments (Imperial Valley), Figure 3 shows thousands of points along roads and canals in

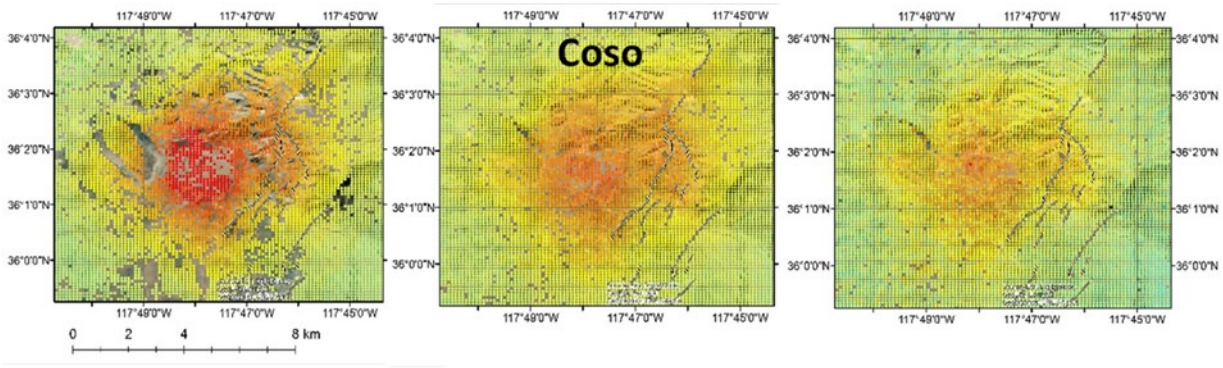

Figure 4. Maps of vertical deformation rates (mm/yr) at Coso obtained from different satellites. Left – ENV, middle – SNT1, right – SNT2. Yellow to red color indicates subsidence. Note decreasing subsidence with time.

the agricultural areas of Imperial Valley. The latter has made it possible to identify deformation amidst these vegetated areas, which would be impossible with early InSAR techniques. Note the interplay of subsidence and uplift changing in time at the HBGF and the decrease with time of the subsidence at Coso. We have shown much more details of these studies in the earlier papers cited above, such as deformation time series, deformation progressions along profiles, and relationship with induced seismicity.

3. PRODUCTION AND INJECTION

Figure 5 shows time series of the total monthly production and injection mass at the four fields. These data were downloaded from the California Geologic Energy Management Division (CalGEM)/California Department of Conservation. The decreasing fluid amounts at Coso and NBGF are associated with the decreasing subsidence observed by InSAR (Eneva et al., 2018; Eneva et al., 2019b) and ground-based surveys at these fields. At Coso, an injection strategy to boost production started in Dec 2009, bringing outside water from

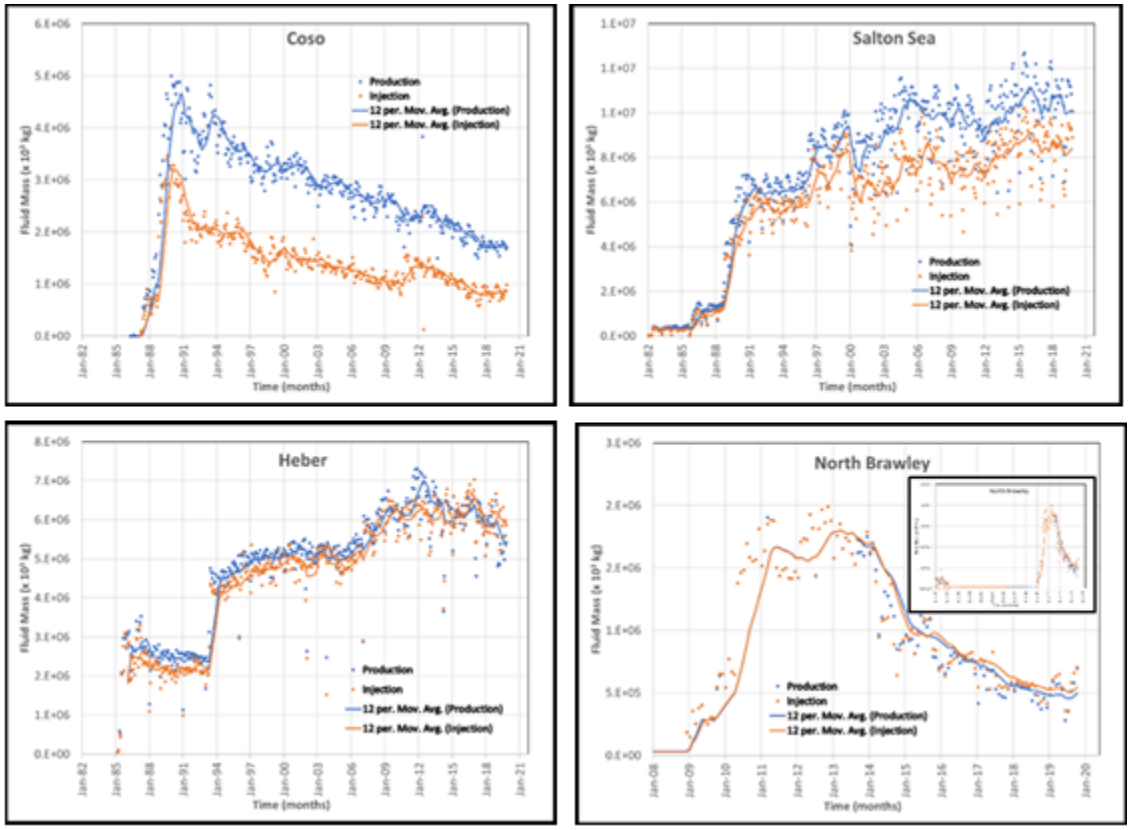

Figure 5. Time series of total monthly production and injection mass from the four geothermal fields. The inset in the North Brawley panel shows a period in the early 80's when a geothermal plant was active for about 5 years before it was decommissioned (Eneva et al., 2019b).

two ranch wells 20 km away. Due to the draught, this injection was suspended temporarily in 2016 for about a year, after which it resumed at a lower level and ended in the fall of 2018 (see the "bump" following 2009 and peaking around 2012 in the Coso plot). At the HBGF, the increase in injection around 2005 when Ormat took over, resulted in a previously subsiding area (known from leveling surveys prior to satellite coverage) to start uplifting (Eneva et al., 2013). The production and injection time series follow each other closely for the HBGF and NBGF due to the binary plants used at these fields. At the SSGF, production has been close to steady for the period 2003-2012 partially covered by ENV observations, with a boost after 2012 due to the start of operation of a new plant (a joint time series is shown for SSGF-CE and SSGF-ES).

4. GROUND-BASED MEASUREMENTS OF SURFACE DEFORMATION

Ground-based subsidence measurements at the Coso geothermal field have been documented in subsidence reports since 1988. These data have been provided by the U.S. Navy Geothermal Program Office (GPO). The second survey was in 1992, followed by four more surveys every year (1993-1996), one survey two years later (2000), and after that, five more surveys every 3-3.5 years (2003, 2006, 2009, 2013, and 2017). The subsidence surveys at Coso started with leveling benchmarks, which were replaced by GPS stations in 1996. The subsidence reports state that the certainty of the ellipsoid heights is between 2 mm and 9 mm at the 95% confidence level, while the mean vertical positional certainty at the 95% confidence level is from ±5.5 mm (earlier reports) to ±3.4 mm (later reports).

In Imperial Valley, the geothermal companies submit annual leveling reports to the Imperial County Department of Public Works (ICDPW), which provided them to us. These reports state that a classical differential leveling technique is used to measure vertical elevations with high order of accuracy. The National Geodetic Survey (NGS) specifications are followed, according to which the minimum accuracy standard of ±6mm * $\sqrt{d}$, for 2nd order class I leveling, with d being the length of section or loop in kilometers, was used in determining allowable tolerances in field error of closure on all sections and loops. All surveys are referenced to local benchmarks (B14 at Coso, S-1246 at SSGF-CE, B-1226 at SSGF-ES, A33 at HBGF, and Y-1225 at NBGF). These datum points were also used to re-reference the InSAR results, so that direct comparisons are possible.

Table 1 shows information for the surveys in the four fields. Figures 6-8 show time series of all available survey data. The Coso plot (Figure 6) shows mostly steady subsidence, as well as decrease in subsidence for most stations after about 2006 (indicated by smaller slopes of the deformation curves). The HBGF plots (Figure 7) show deformation for all stations, as well examples from some stations in the area where subsidence turned to uplift in 2005 and from the area that always exhibits subsidence. Since deformation is measured from the first year of operation of any given benchmark, not all subsidence curves start from 0 at the same times. In Figure 8, the top panels show the decrease of subsidence as production and injection decreased at the NBGF. Some benchmarks were drastically affected by three local moderate earthquakes in Aug 2012 (the largest was M5.4), turning from subsidence to uplift, as marked. Interestingly, continued uplift showed up also in the measurements one year later, in 2013. The bottom panels of Figure 8 show more or less steady subsidence at the SSGF. A number of the benchmarks in the SSGF-CE plot show a jump in subsidence in response to an Aug 2005 M5.1 earthquake that occurred on the territory of this field.

	Coso	SSGF-CE	SSGF-ES	HBGF	NBGF
Period of surveys	Every 1 to 3 yrs Oct 1988-Oct 2017	Annual May 1998-Nov 2018	1992, Annual Dec 2011-Nov 2018	Annual Jan 1994-Dec 2018	Annual Nov 2009-Nov 2018
Number of surveys	13	20	9	25	10
ENV period	2	7	0	6	1
TSX period	n/a	1	2	n/a	2
SNT1 period	1	3	3	3	3
STN2 period	0	1	1	1	1
Number of survey stations/benchmarks	116/73/71	120/119/109	24 in 1992, 95/95/92	138/121/106	80/80/71

Table 1. Information about the ground-based surveys at the four geothermal fields. The last row shows three numbers of stations – used at any time, after satellite coverage started, and at present, respectively.

5. COMPARISON OF DEFORMATION RATES FROM INSAR AND GROUND-BASED SURVEYS

Table 2 shows mean differences and standard deviations of comparisons between the two types of rates for some periods of time. The InSAR results are re-referenced in each case to the locations of the individual datum benchmarks used in the surveys. The InSAR rates are calculated as averages from decomposed vertical measurements within 200 m from the benchmarks. This distance does not have a special meaning – it is a compromise between being close enough to the benchmarks, yet including a representative number of InSAR vertical measurements. The highlighted rows are for differences shown in scatter plots and histograms in Figures 9-12. The scatter plots also show lines and their equations from the application of a least-squares linear fit. Some satellite periods are with very few, or even no surveys at the same time, so comparisons either cannot be made, or rates are calculated from only two or three surveys, with the understanding that such rates are less reliable. Therefore, in order to use data from a few more surveys, the survey periods can be sometimes quite longer than the satellite periods. Also, not all benchmarks have InSAR measurements within 200 m of them, especially

in Imperial Valley where despite of identifying thousands of PS/DS points, there are gaps in coverage in the agricultural areas. If corner reflectors (e.g., Garthwaite et al., 2015) are strategically installed in the future, all benchmarks could have InSAR measurements in their vicinities.

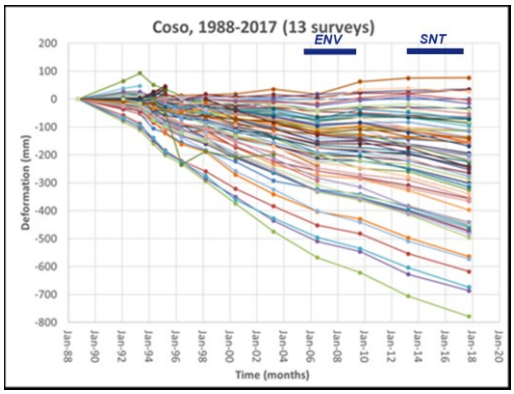

Figure 6. Deformation time series from subsidence surveys carried out at the Coso geothermal field (all stations).

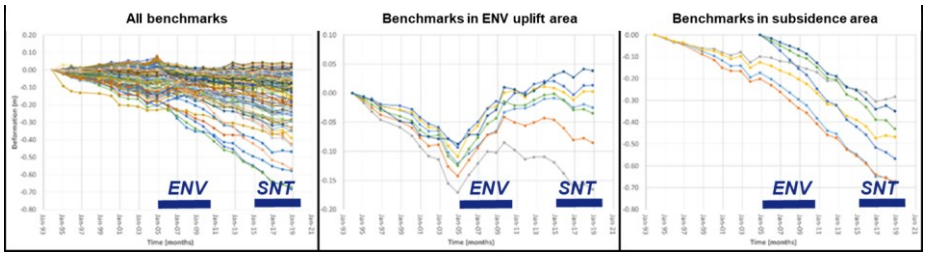

Figure 7. Deformation time series from annual leveling surveys at the Heber geothermal filed. Left – all benchmarks, middle – benchmarks in an area of uplift due to increase in injection in 2005, right - benchmarks in the subsidence area.

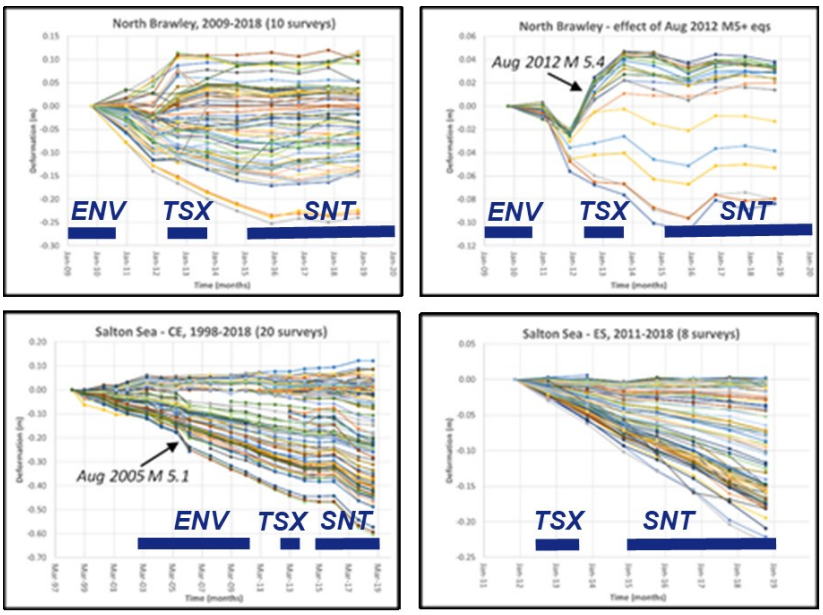

Figure 8. Deformation time series from annual leveling surveys at the Salton Sea and North Brawley geothermal fields. Top left – all benchmarks at NBGF, top right – examples of NBGF time series significantly affected by the M5+ earthquakes in August 2012, bottom left – all benchmarks at the CalEnergy units of the SSGF, bottom right – all benchmarks in the EnergySource area of the SSGF (John L. Featherstone geothermal power plant, formerly known as Hudson Ranch I).

Surv/ Sat	Time intervals	Mean difference, mm/year	95% conf. accuracy, mm/year	Number of surveys	Number of benchmarks	Number of InSAR points in time series
Coso						
S ENV	Apr 2003-Sep 2009 Feb 2006-Aug 2009	0.7 ± 0.3	3.8	3	73 of 73	17 (35 A, 20 D)
S ENV	Jun 2000-Sep 2009 Feb 2006-Aug 2009	2.0 ± 0.2	6.2	4	73 of 73	17 (35 A, 20 D)
S ENV	Apr 2003-Apr 2013 Feb 2006-Sep 2009	0.0 ± 0.3	3.5	4	73 of 73	25 (45 A, 30 D)
S ENV	Jul 2006-Apr 2013 Oct 2006-Sep 2010	–2.2 ± 0.2	5.6	3	71 of 71	23 (30 A, 27 D)
S SNT1	Sep 2009-Oct 2017 Feb 2015-Sep 2017	3.1 ± 0.3	7.4	3	71 of 71	40 (49 A, 46 D)
Salton Sea-CalEnergy						
S ENV	Jun 2004-Feb 2011 Aug 2005-Sep 2010	0.9 ± 0.7	7.2	7	49 of 81	23 (30 A, 40 D)
S ENV	Jun 2004-Mar 2010 Aug 2005-Nov 2009	1.0 ± 0.8	8.7	6	48 of 80	18 (25 A, 34 D)
S SNT1	Mar 2015-Nov 2018 Apr 2015-Apr 2018	6.7 ± 1.2	18.5	4	44 of 113	48 (60 A, 51 D)
S SNT2	Nov 2017-Sep 2019 Jun 2018-Aug 2019	2.8 ± 0.7	14.0	2	82 of 110	36 (37 A, 40 D)
S TSX	Mar 2012-Mar 2014 Sep 2012-Sep 2013	–2.1 ± 0.4	7.4	3	104 of 108	9 (17 A, 15 D)
Salton Sea-EnergySource						
S SNT1	Nov 2014-Nov 2018 Apr 2015-Apr 2018	1.8 ± 0.6	11.8	5	65 of 93	48 (60 A, 51 D)
Heber						
S ENV	Feb 2006-Nov 2010 May 2006-Sep 2010	2.2 ± 0.5	7.3	5	74 of 137	25 (34 A, 30 D)
S SNT1	Dec 2014-Jan 2018 Apr 2015-Dec2017	1.6 ± 0.3	8.3	4	126 of 129	38 (50 A, 41 D)
S SNT2	Dec 2016-Aug 2019 Jun 2018-Aug 2019	2.4 ± 0.5	10.4	3	115 of 127	36 (37 A, 39 D)
North Brawley						
S TSX	Oct 2012-Oct 2013 Oct 2012-Sep 2013	–3.3 ± 1.1	14.5	2	75 of 75	8 (15 A, 12 D)

Table 2. Differences between InSAR vertical rates and rates calculated from the ground-based surveys. Second column - time intervals compared from the surveys (S in the first column) and the satellites (ENV, TSX, SNT1 or SNT2 in the first column). Third column - mean differences and their standard deviations. Fourth column - 95th percentile of the absolute values of the differences. Fifth column - number of surveys used to calculate rates within the survey periods shown in the second column. Sixth column - number of GPS stations (Coso) and benchmarks (Imperial Valley), for which InSAR vertical measurements within 200 m were observed, out of all stations/benchmarks for which rates could be calculated in that period. Last (seventh) column - number of points in the InSAR time series, from which the vertical rates are calculated, followed by the numbers of ascending (A) and descending (D) scenes in parentheses. Rows highlighted in gray are for periods shown in subsequent figures.

For Coso, Table 2 and the top of Figure 9 show that there is a good agreement between the two type of measurements for the survey period Apr 2003 – Sep 2009, with 95% of the absolute values of the differences within 3.8 mm/year. Table 2 shows that the result is similar for the Apr 2003 – Apr 2013 period (not shown in Figure 9). Because the subsidence at Coso decreases with time, when the satellite data period overlaps with the survey period only partially, then a systematic bias is observed. Therefore, the plot on the bottom of Figure 9 shows a systematic positive difference (mean 3.1 ± 0.3 mm/year from Table 2), likely because the SNT1 subsidence rates are generally lower than those derived from the longer period covered by the three surveys in 2009, 2013 and 2017. The reason is that the SNT1 period (Feb 2015-Sep 2017) is in the second half of the survey period (Sep 2009-Oct 2017), when the subsidence is lower. Using a suitably shorter survey period is not possible, because there was only one survey, in Oct 2017, during the SNT1 period.

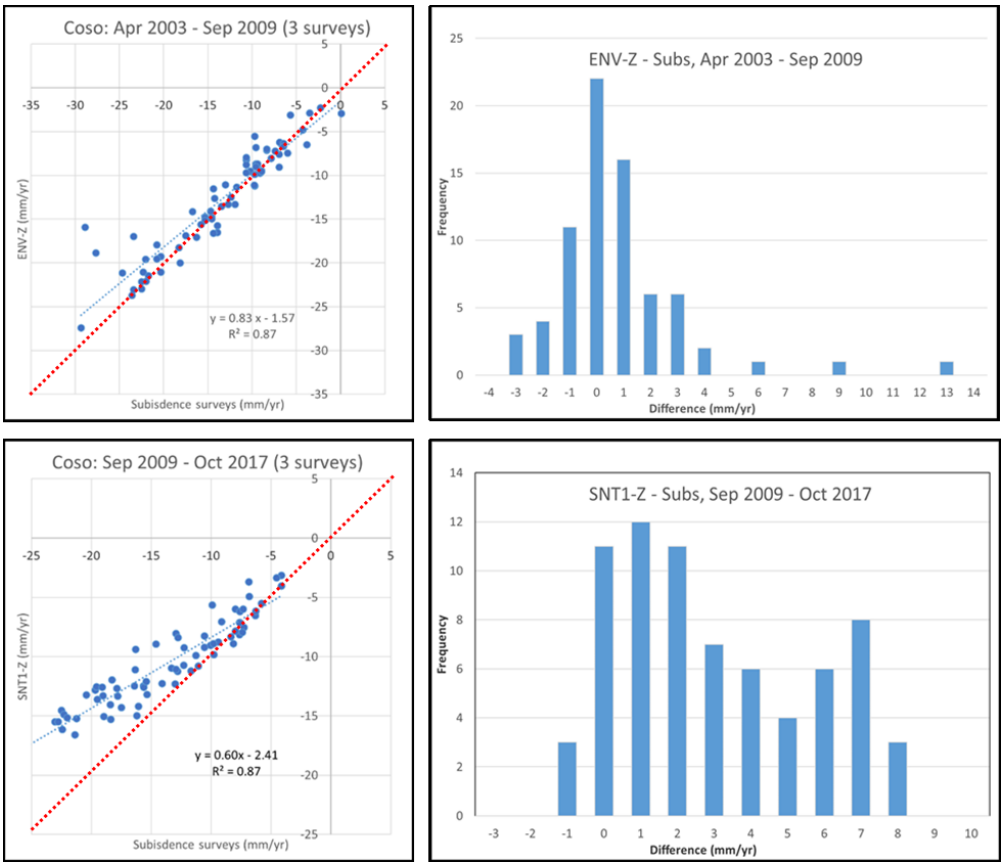

Figure 9. Comparison of annual deformation rates from InSAR (satellites) and ground-based subsidence surveys at the Coso geothermal field. Left – examples of scatter plots for two periods, as indicated, right – corresponding histograms. The dashed red lines show where the points in the scatter plots would be positioned if the survey and InSAR rates were identical.

The results for the Imperial Valley are more variable, which is not surprising in view of the agricultural environment there. Figure 10 shows examples of comparisons of survey rates with ENV and TSX rates for the SSGF-CE. Table 2 shows that in those cases, 95% of the absolute differences are below 7.2 and 7.4 mm/year, respectively, with a tendency for the TSX rates to show larger subsidence, by about −2.1 mm/year on average, than the rates from three leveling surveys encompassing the TSX period. There is a significantly larger bias for the SNT1 period (Table 2) that is not explained at this time and needs further examination. Also, in this case, many benchmarks lack InSAR vertical measurements within a distance of 200 m. Because vertical decomposition is only possible when both types of PS/DS points are identified (descending and ascending), there is loss of information due to ignoring all the numerous LOS measurements when they are of only one type. In particular, in Imperial Valley there are many areas where ascending PS/DS are more abundant than the descending ones, so it may be better in such cases to stay with the LOS measurements and convert the leveling measurements to that LOS direction for comparison purposes. This would identify much more InSAR rates (e.g., ascending LOS rates) within 200 m of the benchmarks, providing a better basis for comparison.

Figure 11 shows results from HBGF for ENV, SNT1 and SNT2. The InSAR vertical rates are by 1.6 to 2.4 mm/year larger than the survey rates (i.e., showing smaller subsidence), and 95% of the absolute values of the differences fall within 7.3 to 10.4 mm/year (Table 2). Finally, Figure 12 displays examples of scatter plots for the SSGF-ES and NBGF, in the ENV and TSX periods, respectively.

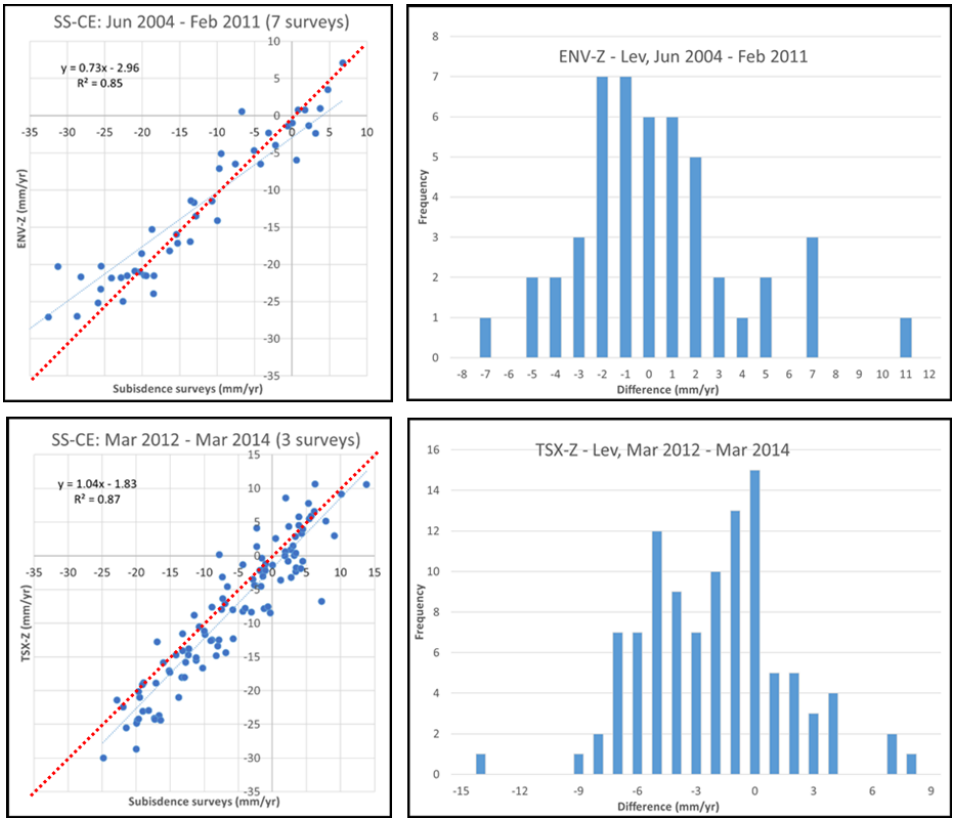

Figure 10. Comparison of annual deformation rates from InSAR and leveling surveys at the CalEnergy units of the SSGF. Left – examples of scatter plots for two periods, right – corresponding histograms. Red dashed lines like in Figure 9.

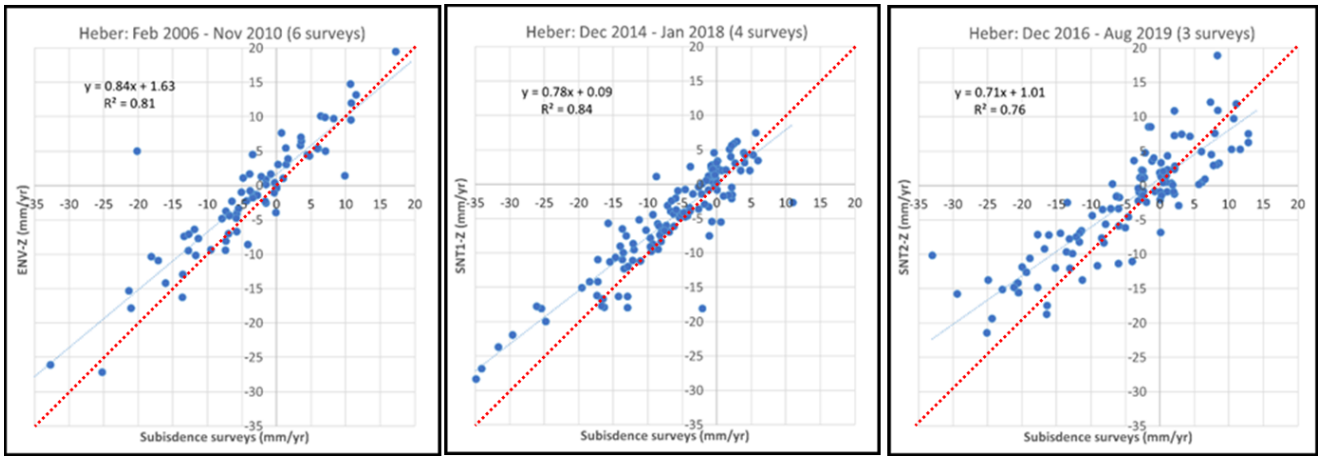

Figure 11. Scatter plots comparing the HBGF annual deformation rates from InSAR and leveling surveys for three periods, as indicated. Red dashed lines like in Figure 9.

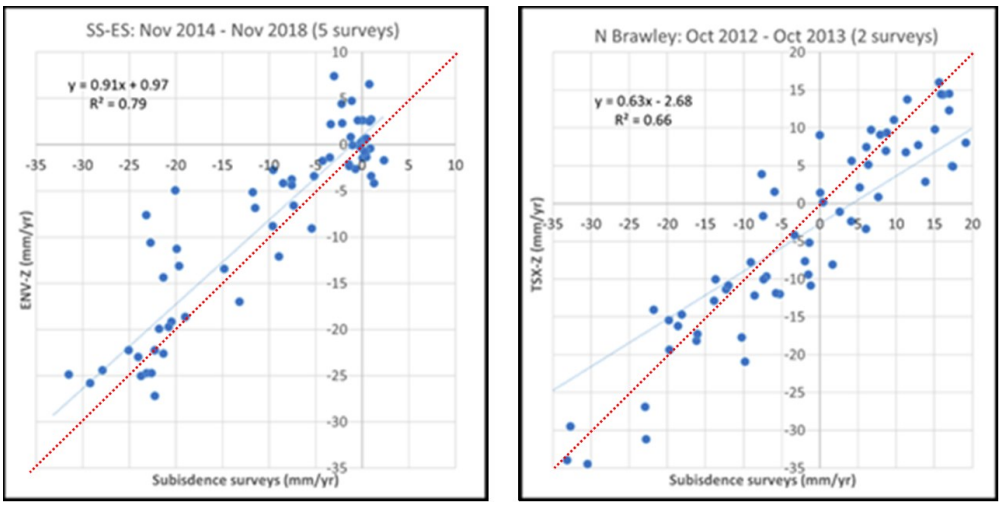

Figure 12. Examples of scatter plots comparing the annual deformation rates from InSAR and leveling surveys for the EnergySource part of SSGF (left) and for NBGF (right). Red dashed lines like in Figure 9.

The results of these comparisons indicate that for the most part, the two types of measurements agree reasonably well with each other. However, there are some systematic biases, and the scatter is sometimes substantial, limiting the conclusions for individual benchmarks, especially for the SNT1 period at SSGF-CE. Still, on average, the differences are small enough that the overall spatial patterns of surface deformation derived from InSAR and the ground-based surveys should be similar.

A study from the Department of Water Resources/California Natural Resources Agency, for which TRE Altamira Inc. provided InSAR measurements, compared InSAR deformation with measurements from continuous GPS in more than 200 groundwater basins in California (*InSAR Data Accuracy*, 2019). The conclusion was that InSAR using Sentinel data in the period Jan 2015 − Jun 2018 measured vertical displacement in California within 16-mm accuracy, at the 95% confidence level. The report stated that this is valid for the state-wide data set, and results may be different for regional and localized area data subsets. Obviously, the annual surveys here are very different in collection frequency compared with the continuous GPS used in that study. However, the accuracy stated is comparable with the numbers listed in the fourth column of Table 2 above (95% percentile of the absolute differences). We cannot make suitable comparisons with continuous GPS stations, because they are outside the geothermal fields studied here.

6. CONCLUSIONS

We carried out comparisons of surface deformation rates derived from satellite data using InSAR and from ground-based surveys at four geothermal fields in California – Coso, Salton Sea, Heber, and North Brawley. Data from three satellites were used for InSAR − Envisat, Sentinel, and TerrSAR-X. The survey data are collected every 3-3.5 years at Coso, and annually at the three other fields. When the periods with satellite data and survey measurements closely match, average differences are for the most part within 3.5 mm/year, with standard deviations of up to 1.2 mm/year. In some cases, the differences are much smaller. These rates are reasonably close on average, so that spatial patterns of deformation based on the two types of measurements are similar.

7. ACKNOWLEDGMENTS

This work is part of a project funded by the California Energy Commission (GRDA grant GEO-16-003), with Elisabeth de Jong as a technical manager. The U.S. Navy Geothermal Program Office has provided the data from the subsidence surveys at the Coso geothermal field. The Imperial County Department of Public Works has continued to support our work by providing reports on the annual leveling surveys at the geothermal fields in Imperial Valley.

REFERENCES

Blake, K., Sabin, A., Eneva, M., Nale, S., Lazaro, M., Tiedeman, A., Meade, D., and Huang, W.-C.: Updated Shallow Temperature Survey and Resource Evolution for the Coso Geothermal Field, *Proceedings of World Geothermal Congress, April 2020* (submitted).

Barbour, A.**,** Evans, E., Hickman, S., and Eneva, M: Subsidence Rates at the Southern Salton Sea Consistent with Reservoir Depletion, *Journal of Geophysical Research: Solid Earth,* **121**, (2016), 5308-5327.

California Geologic Energy Management Division (CalGEM)/California Department of Conservation – last accessed January, 2020, https://www.conservation.ca.gov/calgem.

Eneva, M., Adams, D., Hsiao, V., Falorni, G., and Locatelli, R.: Surface Deformation at the Heber Geothermal Field in Southern California, *Proceedings of the 44th Workshop on Geothermal Reservoir Engineering Stanford University*, Stanford, California, February 11-13, (2019a), SGP-TR-214.

Eneva, M., D. Adams, G. Falorni, and M. Shumski: Surface Deformation and Seismicity at the North Brawley Geothermal Field in Southern California, *Geothermal Resources Council Transactions* **43**, (2019b), 767-783.

Eneva, M., Barbour, A., Adams, D., Hsiao, V., Blake, K., Falorni, G., and Locatelli, R.: Satellite Observations of Surface Deformation at the Coso Geothermal field, California, *Geothermal Resources Council Transactions*, **42**, (2018), 1383-1401.

Eneva, M., Adams, D., Falorni, G., Novali, F., and Hsiao, V.: Surface Deformation at the Salton Sea Geothermal Field from High-Precision Radar Interferometry, *Geothermal Resources Council Transactions*, **38**, (2014), 991-999.

Eneva, M., Adams, D., Falorni, G., and Morgan, J.: Applications of Radar Interferometry to Detect Surface Deformation in Geothermal Areas of Imperial Valley in Southern California, *Proceedings,* 38th Workshop on Geothermal Reservoir Engineering, Stanford University, Stanford, CA (2013a), SGP-TR-198.

Eneva, M., Adams, D., Falorni, G., and Morgan, J.: Application of Radar Interferometry to Detect Subsidence and Uplift at the Heber Geothermal Field, Southern California, *Geothermal Resources Council Transactions*, **37**, (2013b), 491-499.

Eneva, M., Adams, D., Falorni, G., and Morgan, J.: Surface Deformation in Imperial Valley, CA, from Satellite Radar Interferometry, *Geothermal Resources Council Transactions*, **36**, (2012), 1339-1344.

Eneva, M., Falorni, G., Adams, D., Allievi, J., and Novali, F.: Application of Satellite Interferometry to the Detection of Surface Deformation in the Salton Sea Geothermal Field, California, *Geothermal Resources Council Transactions*, **33**, (2009), 315-319.

Ferretti, A., Fumagalli, A., Novali, F., Prati, C., Rocca, F., and Rucci, A.: A New Algorithm for Processing Interferometric Data-Stacks: SqueeSAR." *IEEE Trans. Geosc. Remote Sensing*, **49**(9), (2011), 3460-3470.

Garthwaite, M., Sarah Lawrie, S., Dawson, J., and Thankappan, M.: Corner Reflectors as Tie Between InSAR and GNSS Measurements: Case Study of Resource Extraction in Australia, *Proceedings*, Fringe Workshop, Frascati, Italy, (2015), ESA SP-731.

InSAR Data Accuracy for California Groundwater Basins: CGPS Data Comparative Analysis, January 2015 to June 2018, California Department of Water Resources, Prepared by Towill Inc., with the participations of TRE Altamira Inc. (2019), pp. 159.

Sarychikhina, O., Glowacka, E., Mellors, R., and Suarez, V.F.: Land Subsidence in the Cerro Prieto Geothermal Field, Baja California, Mexico, from 1994 to 2005. An Integrated Analysis of DInSAR, Leveling, and Geological Data, *Journal of Volcanology and Geothermal Research*, **204**, (1-4), (2011), 76-90, doi: 10.1016/j.jvolgeores.2011.03.004.